# Modeling Carmustine Diffusion from Gliadel® Wafers in the Brain to Optimize Cancer Treatment and Minimize Damage to Healthy Tissue

Group 3
Julian Azar, Joshua Elacqua, David Peñaranda, Alexander Stone

BEE 4530: Computer-Aided Engineering
Applications to Biomedical Processes

Spring 2016

**Table of Contents**

## 1: Introduction to Gliadel® Wafers and Our Model

Gliadel® wafers have been developed to circumvent traditional obstacles in brain cancer treatment. Chemotherapeutic drugs administered intravenously are rendered largely ineffective by the blood-brain barrier. Gliadel wafers can be implanted at the tumor removal site during surgery. These wafers then secrete carmustine (also commonly referred to as BCNU) directly into the remaining tumor tissue. Treatment via Gliadel wafers has been widely successful. However, treatment using carmustine can also cause a variety of serious side effects.

Thus, we developed a model to examine the efficacy of Gliadel wafers and improve administration of carmustine to the tumor while minimizing damage to healthy tissue and the occurrence of harmful side effects. The transient diffusion of carmustine from wafers in a realistic, three-dimensional brain geometry was examined using COMSOL®. A zero flux boundary condition was used to represent the blood-brain barrier. Blood flow in the brain and degradation of the drug in both the tumor layer and healthy brain tissue were also considered. Optimal wafer properties were then determined to achieve high carmustine concentrations in the leftover tumor and low concentrations in the healthy tissue.

## 2: Background – Gliomas and Chemotherapy

*Glioma* refers to tumors of the glial cells in the central nervous system (Holland, 2000). Gliomas can be divided into four grades, with glioblastoma multiforme (GBM), grade 4, being the most aggressive and fatal grade. This grade also happens to be the most common in humans. Most patients die within a year of developing GBM and very few survive long-term. This is due, in part, to the difficulties of treating the disease. Complete tumor resection is not feasible – a typical surgery is only able to remove up to 90% of the tumor – and gliomas are resistant to traditional intravenous chemotherapy due to the blood-brain barrier (Holland, 2000).

In order to overcome these problems, Gliadel® wafers have been used. These wafers are implanted in the resection cavity after surgical removal of the tumor. They secrete the chemotherapeutic compound carmustine (BCNU) directly into the tumor region, resulting in the growth inhibition and death of the remaining tumor cells. This method has met with success in recent years (Dyke, et al., 2007). The currently proposed mechanism of carmustine action is inhibition of glutathione reductase resulting in the accumulation of reactive oxygen species and apoptosis (An, et al., 2011). However, exposure to large doses of carmustine can cause serious side effects in patients including seizures, intracranial hypertension, impaired neurosurgical wound healing, and meningitis (RxList, 2013). Thus, maximizing the positive effects of carmustine, while minimizing its negative side effects, should prove fruitful.

During surgery, Gliadel wafers are placed in the region from which the tumor was partially resected. These wafers are thin, cylindrically-shaped slabs that are placed in a relatively uniform manner around the region. Each wafer contains an initial concentration of carmustine and is degraded over time to release the drug into the surrounding tumor area (Teo, et al., 2005).

## 3: Literature Review

In a large clinical trial performed by Westphal, et al. (2006), the use of Gliadel was shown to increase the longevity of patients suffering from malignant gliomas. Median patient survival time was extended from 11.6 to 13.8 months. Patients also had significant survival advantages after two and three years when treated with Gliadel. Another study (Panigrahi and Parikh, 2011) showed that the usage of Gliadel wafers with 7.7 mg of carmustine increased the mean survival time to 21 months when, treatment-free, a patient would be expected to die within a year.

Although Gliadel has shown promising results in halting tumor growth within the brain, case studies have demonstrated negative aspects of it. For example, the use of Gliadel wafers has led several patients to experience edema in the brain, as well as ventricular shift (Weber and Goebel, 2005). A separate study has shown that Gliadel wafer implantation after surgery causes seizures in at least a third of patients (Panigrahi and Parikh, 2011). Thus, it is crucial to continue researching ways to minimize these negative effects.

## 4: Problem Statement

Currently, there are no acceptable models of carmustine diffusion from Gliadel wafers into cancerous tissue leftover after resection. Some present models are inaccurate due to their use of fewer than three dimensions and over-simplification of brain blood flow. Our model solves these issues.

## 5: Design Objectives (Goals)

Our work uses COMSOL® to model three-dimensional mass transfer with a domain composed of the Gliadel wafers, the tumor region, and healthy brain tissue. For simplification, the wafers in the model are approximated as a layer as seen in Figure 1. After creating the model, wafer properties were altered to optimize carmustine distribution for treating the tumor region and protecting healthy tissue. A threshold carmustine concentration must be achieved in the tumor region to ensure drug efficacy, while concentration in the healthy tissue should be minimized to reduce harmful side effects.

This model of carmustine diffusion from Gliadel wafers had two objectives. First, an accurate, three-dimensional representation of the diffusion dynamics of carmustine within the brain was generated. To create an accurate model, we retrieved an image of the lateral side of the brain from the internet (Kenhub, 2016), used ImageJ to turn it into a binary (black and white) image, used the ImageJ “edges” command to get the outline, saved the outline as an image, and used img2CAD to turn the outline image from the pixel format to the vector format (*.dxf). We uploaded our final image in COMSOL and extruded it to obtain our three dimensional geometry. Models of carmustine diffusion have been previously created (Brennan, et al., 2009; Brendel, et

al., 2013); however, many of these have been inaccurate due to the use of unrealistic geometries in lower dimensions.

Second, we modeled a potential solution to minimize the negative effects of the drug on the healthy tissue within the brain. An ideal wafer would diffuse carmustine only to the specific areas affected by cancer. However, this is physically unrealistic, and thus efforts must be taken to mitigate diffusion to healthy tissue as much as possible.

**6: Schematic of the Brain Model**

We created a 3D brain geometry to use as our computational domain. Shown in Figure 1 is a 2D schematic representation of a cross-section of the domain using the average dimensions of a human brain. The average thickness, which extends into the page and isn't shown, is 140 mm. A portion of 3 cm radius is removed to represent the resected tumor. Since most brain tumors are not completely removed in surgery, a 4 mm thick tumor layer remains (shown in grey) (Chudler, 2016). A Gliadel wafer layer (shown in blue) is located on top of the tumor layer. For simplification, we model the wafers as a uniform layer instead of eight individual domains. Additionally, fluid will fill the resection cavity post-surgery. Carmustine molecules (shown in yellow) then diffuse out of the wafers and into the tumor layer and healthy brain tissue (shown in pink). We have also included an image of the full COMSOL representation of our geometry and a zoomed-in view of the tumor area (Figure 4).

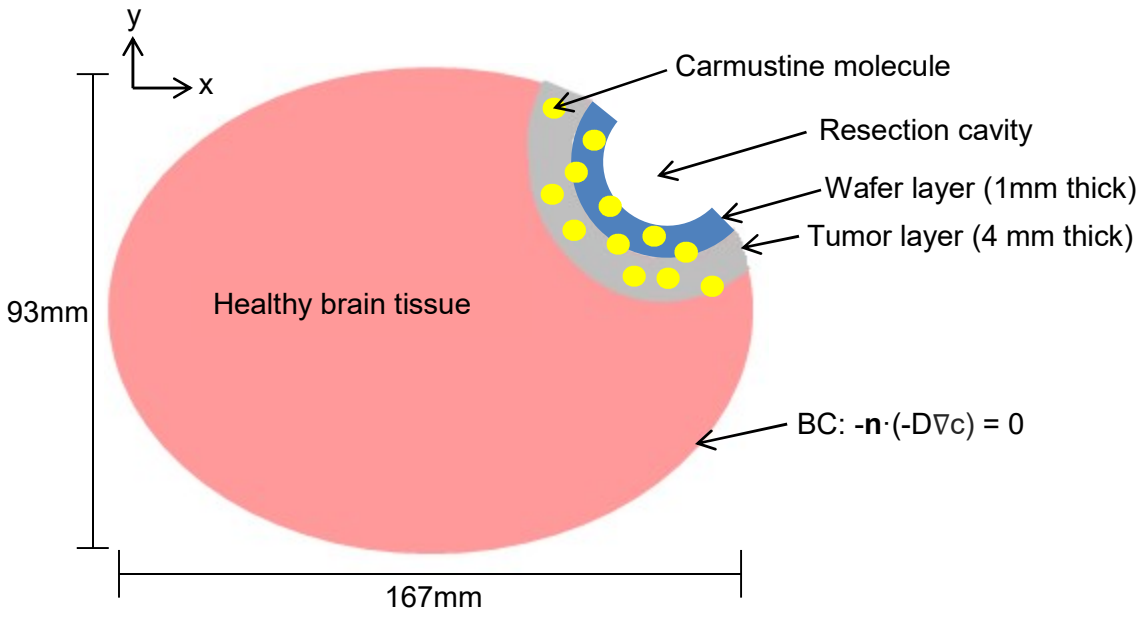


**Figure 1:** A two-dimensional schematic of the modeled drug transfer process. All necessary brain dimensions for this model have been included.

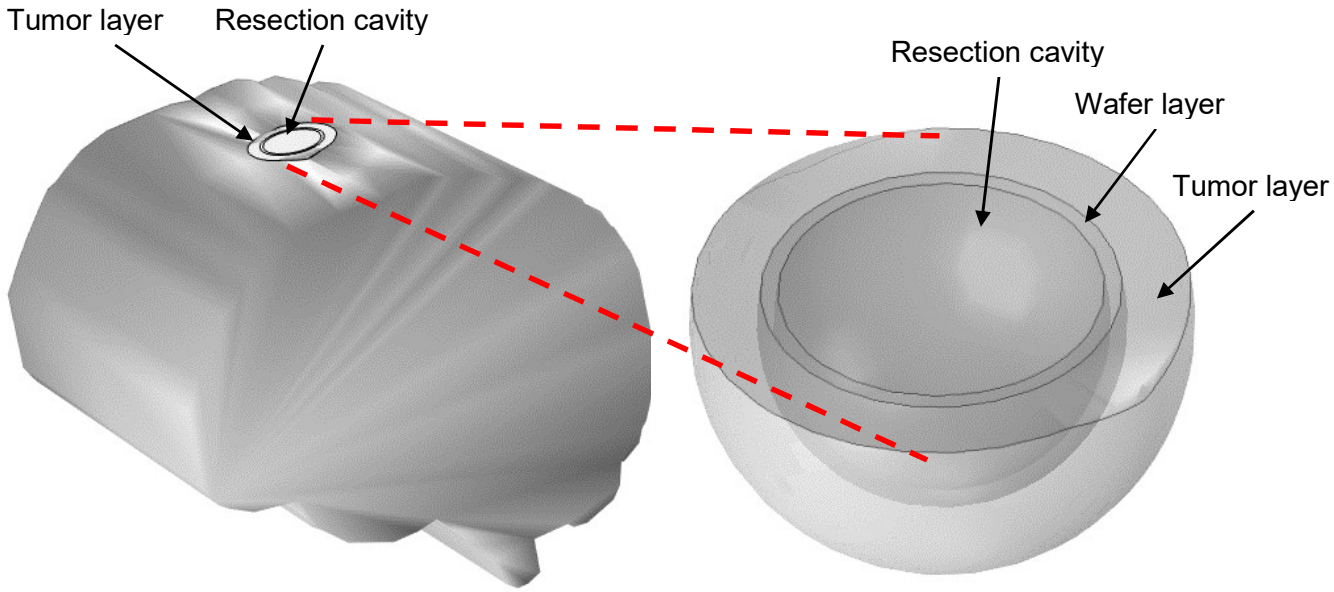


**Figure 2: Left -** Image of the smoothed out brain geometry to be used for modeling in COMSOL. The tumor layer and resection cavity are labelled. The wafer layer is in between the tumor and cavity, but is not labelled due to its small size. The brain is 167 mm long, 140 mm wide, and 93 mm high. **Right** – Zoomed-in view of the tumor region to make the wafer layer more visible. The tumor layer is 4 mm thick with an outer radius of 15 mm and the wafer layer is 1 mm thick.

## 7: Governing Equations – Carmustine Diffusion and Blood Flow

The diffusion of carmustine is transient and involves consumption of the drug. Convection resulting from blood flow in the brain should also be taken into account. Thus, the governing equation for mass transport is as shown below in Equation 1 (Teo, et al., 2005).

$$\frac{dc}{dt} + \nabla \cdot (\boldsymbol{v}c) = \nabla \cdot (D\nabla c) - R + F_s - F_{ls} \quad (1)$$

The parameters $F_s$ and $F_{ls}$ represent drug gain from blood capillaries and loss to lymphatic vessels, respectively. Since the brain does not contain a well-defined lymphatic system, we will approximate $F_{ls}$ to zero and our governing equation becomes Equation 2. The drug degradation rate (R) and $F_s$ are represented by Equations 3 and 4 (Teo, et al., 2005).

$$\frac{dc}{dt} + \nabla \cdot (\boldsymbol{v}c) = \nabla \cdot (D\nabla c) - R + F_s \tag{2}$$

$$R = \begin{cases} \beta_c c & in\ the\ cavity \\ 0 & in\ the\ wafer \\ \frac{V_{\max} c}{k_m + c} + k_e c \approx \frac{V_{max}}{k_m} c + k_e c & in\ the\ tissues \end{cases} \tag{3}$$

$$F_s = \begin{cases} 0 & in\ the\ cavity \\ S_0 e^{-\frac{t}{\tau}} & in\ the\ wafer \\ F_v(1-\sigma)c_v + \frac{\delta S}{V}(c_v - c)\left(\frac{Pe_v}{e^{Pe_v}-1}\right) & in\ the\ tissues \end{cases} \tag{4}$$

$K_e$, and Pev represent the non-enzymatic elimination constant and the trans-capillary Peclet number, respectively (Teo, et al., 2005).

$$k_e = \frac{\ln(2)}{t_{1/2}} \tag{5}$$

$$Pe_v = \frac{F_v(1-\sigma)}{\delta S/V} \tag{6}$$

The governing equations that define the fluid flow in the brain are the continuity equation shown in Equation 7 and flow through porous media shown in Equation 8. Blood is considered to be incompressible (Teo, et al., 2005).

$$\nabla \cdot \boldsymbol{v} = \begin{cases} F_v - F_{ls} = F_v & in\ the\ tissues \\ 0 & elsewhere \end{cases} \tag{7}$$

$$\frac{d(\rho v)}{dt} + \nabla \cdot (\rho \boldsymbol{v}\boldsymbol{v}) = \rho \boldsymbol{g} - \nabla P_i + \nabla \cdot \Gamma + \theta \mu \boldsymbol{v} + \frac{\rho}{2} \Psi |\boldsymbol{v}| \boldsymbol{v} \tag{8}$$

The fluid source, $F_v$, is modelled in Equation 9 by Starling's Law (Teo, et al., 2005).

$$F_v = \frac{K_v S}{V}\left(P_v - P_i - \sigma_T(\pi_v - \pi_i)\right) \tag{9}$$

*7.1: Physical Parameters and Constants*

The diffusivities of carmustine in the resection cavity, wafers, tumorous tissue, and healthy tissue are summarized below in table 1 (Teo, et al., 2005).

**Table 1:** Diffusivity in all regions of the brain to be modeled.

| Region | Diffusivity ($m^2/s$) |
|---|---|
| Cavity | $1.43 \times 10^{-9}$ |
| Gliadel Wafer | $2.0 \times 10^{-12}$ |
| Tumor | $6.75 \times 10^{-9}$ |
| Healthy Tissue | $2.5 \times 10^{-10}$ |

All required material properties and physical constants used in the above equations are summarized below in Table 2. The average tumor pressure, $P_i$, initially changes with time, but quickly reaches a steady state value after two hours. Since our model represents significantly longer than two hours of real time, we will assume $P_i$ always has its steady state value.

**Table 2:** Necessary material parameters and physical constants.

| Parameter | Definition | Value | Reference |
|---|---|---|---|
| $\beta_c$ | Degradation rate in cavity | $6.67 \times 10^{-4}\ \mathrm{s}^{-1}$ | Loo, et al., 1966 |
| $k_c$ | Permeability in the cavity | $3.564 \times 10^{-10}\ \mathrm{m}^2$ | Teo, et al., 2005 |
| $V_{max}$ | Michaelis-Menten parameter | $1.7 \frac{\mathrm{nmol}}{\mathrm{mg\ protein} * \mathrm{min}}$ | Levin, et al., 1978 |
| $k_m$ | Michaelis-Menten parameter | $625 \frac{\mu\mathrm{mol}}{\mathrm{mg\ protein}}$ | Levin, et al., 1978 |
| $t_{1/2}$ | Half-life of carmustine | 90 min | Goodman, et al., 1990 |
| $S_0$ | Fitted parameter, source from wafer | $5.659 \times 10^{-4} \frac{\mathrm{kg}}{\mathrm{m}^3\mathrm{s}}$ | Teo, et al., 2005 |
| $\tau$ | Fitted parameter, time constant | $1.667 \times 10^5\ \mathrm{s}$ | Teo, et al., 2005 |
| $\sigma$ | Osmotic reflection coefficient for carmustine | 0.82 in tumor region | Baxter and Jain, 1989 |
| | | 0.91 in healthy tissue | |
| $\delta$ | Vascular permeability | $8.31 \times 10^{-5} \frac{\mathrm{m}}{\mathrm{s}}$ in tumor region | Baxter and Jain, 1989 |
| | | $1.06 \times 10^{-5} \frac{\mathrm{m}}{\mathrm{s}}$ in healthy tissue | Saltzman and Radomsky, 1991 |
| S/V | Exchange area of blood vessels per unit tissue | $20000\ \mathrm{m}^{-1}$ in tumor region | Baxter and Jain, 1989 |
| | | $7000\ \mathrm{m}^{-1}$ in healthy tissue | |
| $c_v$ | Carmustine concentration in blood | 0 | Teo, et al., 2005 |
| $\rho$ | Interstitial fluid density | $1000 \frac{\mathrm{kg}}{\mathrm{m}^3}$ | Perry, 1997 |
| g | Gravitational constant | $-9.81 \frac{\mathrm{m}}{\mathrm{s}^2}$ | Teo, et al., 2005 |
| $P_i$ | Average tumor pressure | 1000 Pa | Teo, et al., 2005 |
| $\Gamma$ | Stress tensor | n.a. | n.a. |
| $\theta$ | Viscous loss | n.a. | n.a. |
| $\mu$ | Interstitial fluid viscosity | $0.78 \times 10^{-3}\ \mathrm{Pa} * \mathrm{s}$ | Perry, 1997 |
| $\Psi$ | Inertial loss | n.a. | n.a. |
| $P_v$ | Vascular pressure | 2080 Pa | Baxter and Jain, 1989 |
| $\pi_i$ | Osmotic pressure of interstitial fluids | 2000 Pa in tumor region | Baxter and Jain, 1989 |
| | | 1330 Pa in healthy tissue | |
| $\pi_v$ | Osmotic pressure of plasma fluids | 2660 Pa | Baxter and Jain, 1989 |
| $k_v$ | Hydraulic conductivity of microvascular wall | $2.11 \times 10^{-11} \frac{\mathrm{m}^2\mathrm{s}}{\mathrm{kg}}$ in tumor region | Baxter and Jain, 1989 |
| | | $2.7 \times 10^{-12} \frac{\mathrm{m}^2\mathrm{s}}{\mathrm{kg}}$ in healthy tissue | |

## 8: Boundary Conditions

Since our system consists of the resection cavity, wafers, and the brain, the primary boundary for drug diffusion is the edge of the brain. Due to the blood-brain barrier, there is a zero flux condition at this edge. Additionally, we assumed that there is no drug flow out of the top of the cavity. These boundary conditions can be observed above, on Figure 1.

Additionally, we used zero flux conditions on all boundaries of the brain tissue while modelling fluid flow. To do this, we assumed that no blood is lost from the system.

## 9: Initial Conditions

In the wafers, the initial concentration of carmustine was modeled as zero. Instead of using an initial condition, we used a source term to represent carmustine being released over time as the biodegradable wafer matrix is eroded away (Teo, et al., 2005).

The initial carmustine concentration in the cavity, tumor region, and healthy brain tissue was zero. No drug is present in the brain prior to insertion of the wafers.

For fluid flow, we used a zero velocity initial condition.

## 10: Results

### *10.1: Mesh Convergence*

After creating the appropriate geometries in COMSOL, we were able to perform mesh convergence on concentration and average fluid velocities at a cut point in the middle of the tumor layer (Figure 3).

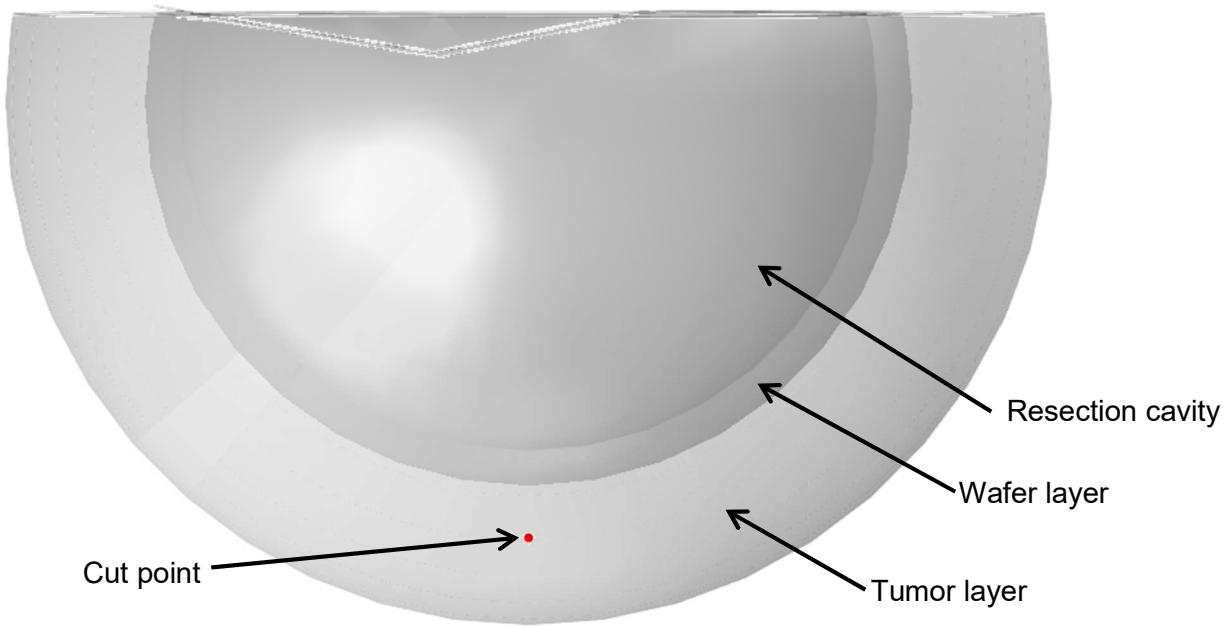


**Figure 3:** Cut point in the tumor layer used to perform mesh convergence in COMSOL.

These convergences were performed in an uncoupled manner. As can be seen in Figure 4, the mesh has converged for carmustine concentration by 55,758 elements, when increasing the number of elements caused the average concentration of carmustine to fluctuate about a concentration of $2.9\times10^{-5}$ kg/m$^3$. The mesh appears to always be converged for fluid velocity as the result after 72 hours is always the same, regardless of the mesh. A converged mesh with 83,068 elements is shown below in Figure 5. The tumor and wafer layers of our geometry require smaller mesh elements than the healthy brain region since this area experiences the highest degree of mass flux.

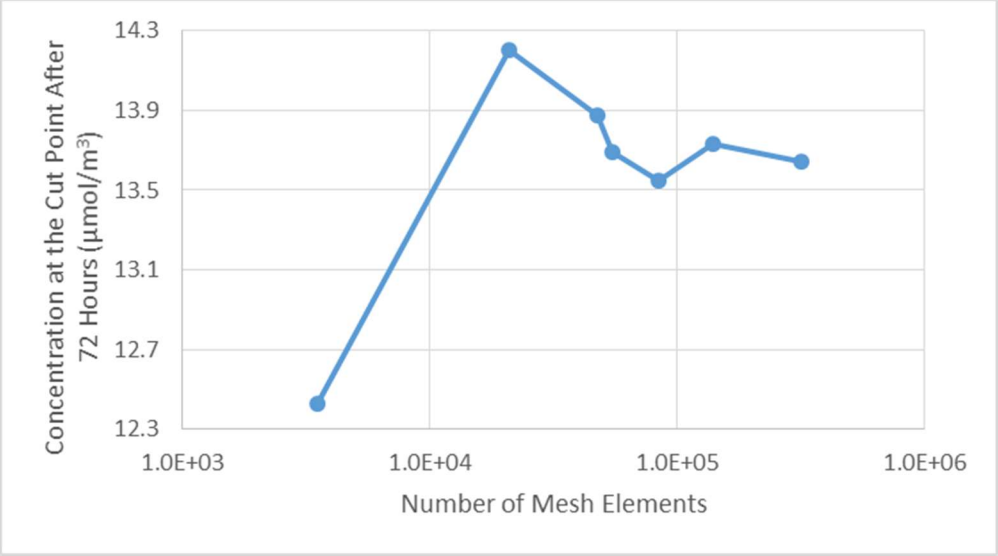


**Figure 4:** Mesh convergence plot. Carmustine concentration in the tumor layer after 72 hours was recorded for increasingly refined meshes until refining the mesh further ceased to change the solution.

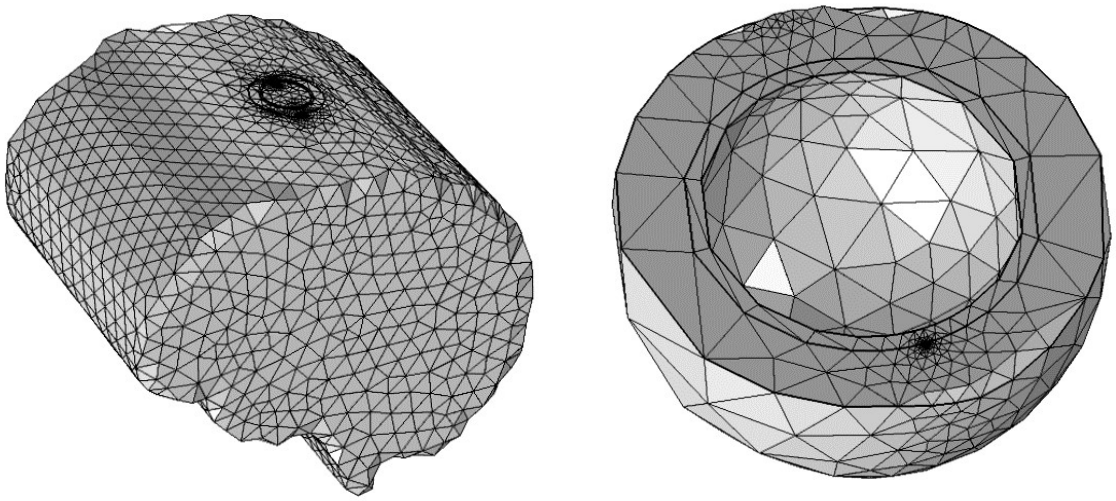

**Figure 5:** Converged mesh used for modelling. On the left is a zoomed out image of our whole mesh. On the right, only the tumor and wafer layers are included to better show the smaller mesh elements around the tumor region and wafers. The mesh elements need to be finer in this area as it is where most of the drug diffusion will be occurring.

*10.2: Drug Concentration Over Time*

Running a simulation of length 72 hours using our converged mesh, we received the below slice plots of carmustine concentrations throughout the brain. Figure 6 shows what we would expect for drug concentration in the wafers. Concentration can be shown to increase at a rapid rate initially and then decrease over time.

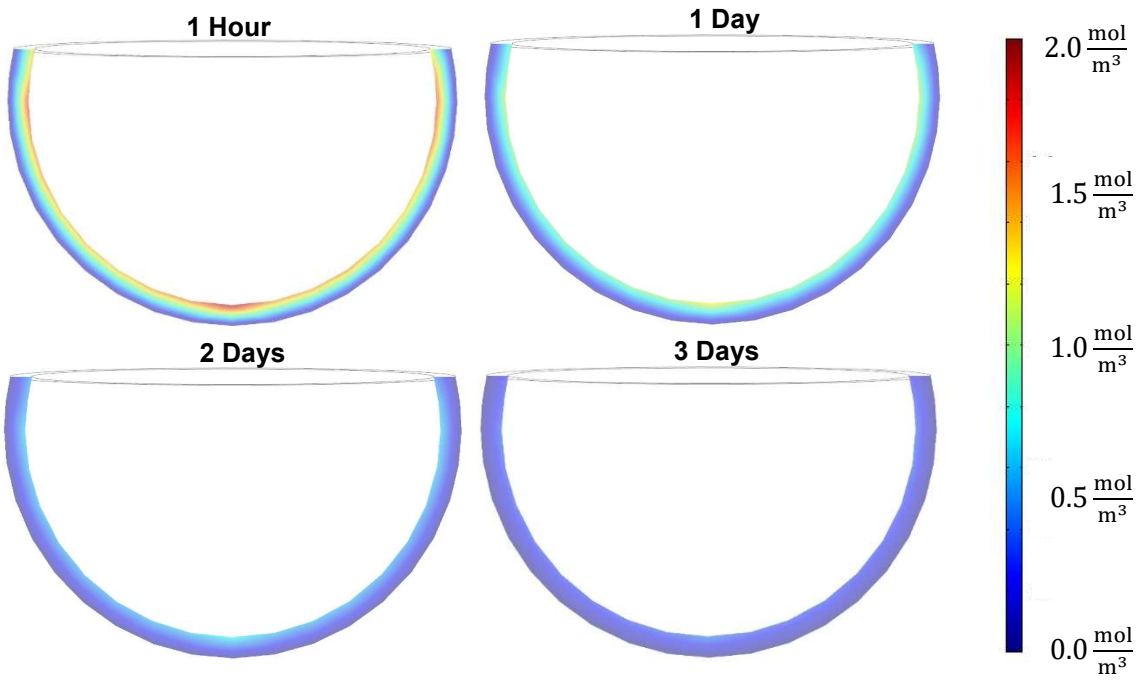


**Figure 6:** Drug concentration in the wafer one hour, one day, two days, and three days post-implantation. Carmustine rapidly increases in concentration just after implantation and then slowly decreases as time goes on and the drug diffuses into the surrounding tissue. After three days, most of the carmustine has left the wafers.

Figure 7 shows the carmustine concentrations in the tumor layer of the brain over the 72 hour period. Carmustine can be seen to quickly build up in the tumor region and slowly decline in concentration over time, reaching a maximum concentration of $3.5 \times 10^{-3}$ mol/m$^3$. Unfortunately, these plots show that COMSOL's computation has resulted in the model containing a small unphysical region. A small area of the tumor region appears to have negative carmustine concentrations, which is physically impossible. This error arises due to the numerical limitations of a computer and the inaccuracies associated with finite element computations.

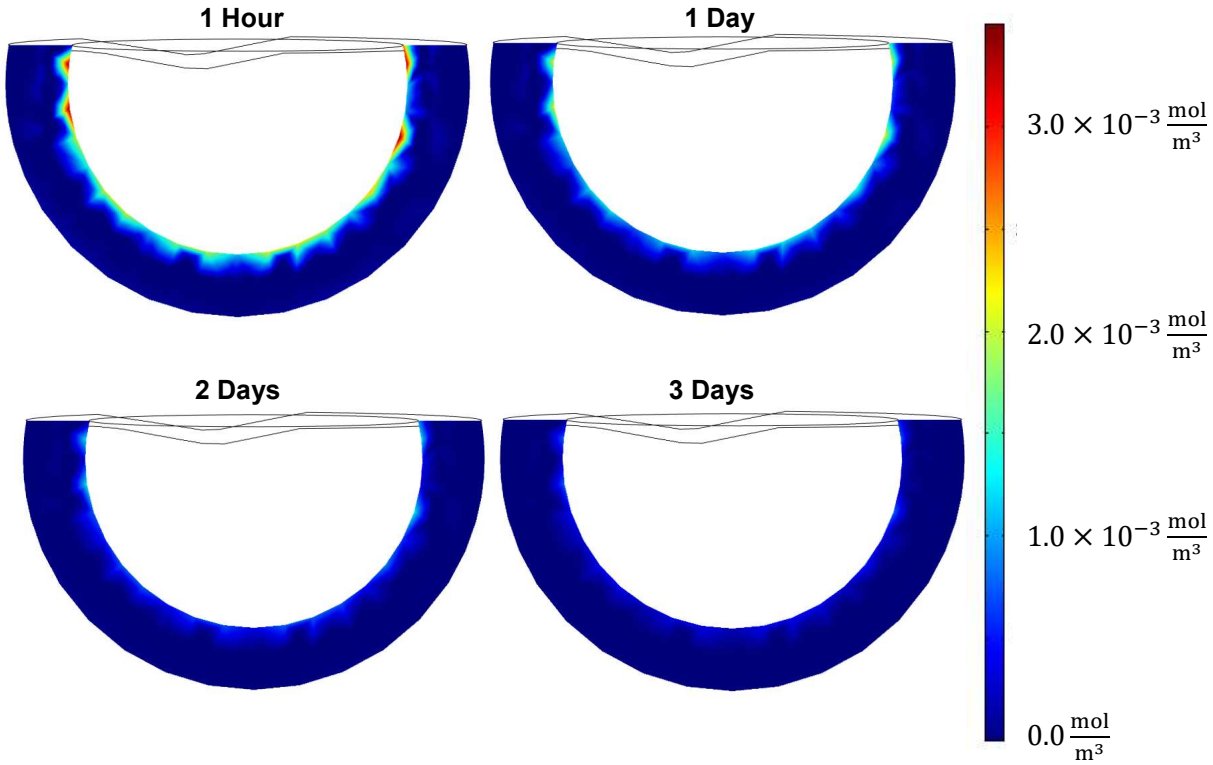


**Figure 7:** Drug concentration in the tumor layer one hour, one day, two days, and three days post-implantation. Carmustine builds up in the tumor region to kill the cancerous tissue and remains present, but at declining concentrations, over the course of three days.

The drug is able to diffuse through the whole tumor layer and into the healthy brain tissue, as shown in Figure 8. Very little drug is actually able to diffuse to the healthy tissue before being degraded, causing the carmustine to be localized in a region just around the tumor layer reaching a maximum concentration of $1.5 \times 10^{-4}$ mol/m$^3$. Most of the healthy tissue contains negligible concentrations of carmustine. Of note, like the tumor region, the healthy brain tissue also displays a small area where the carmustine concentration is unphysical. It occurs for the same reasons in both regions.

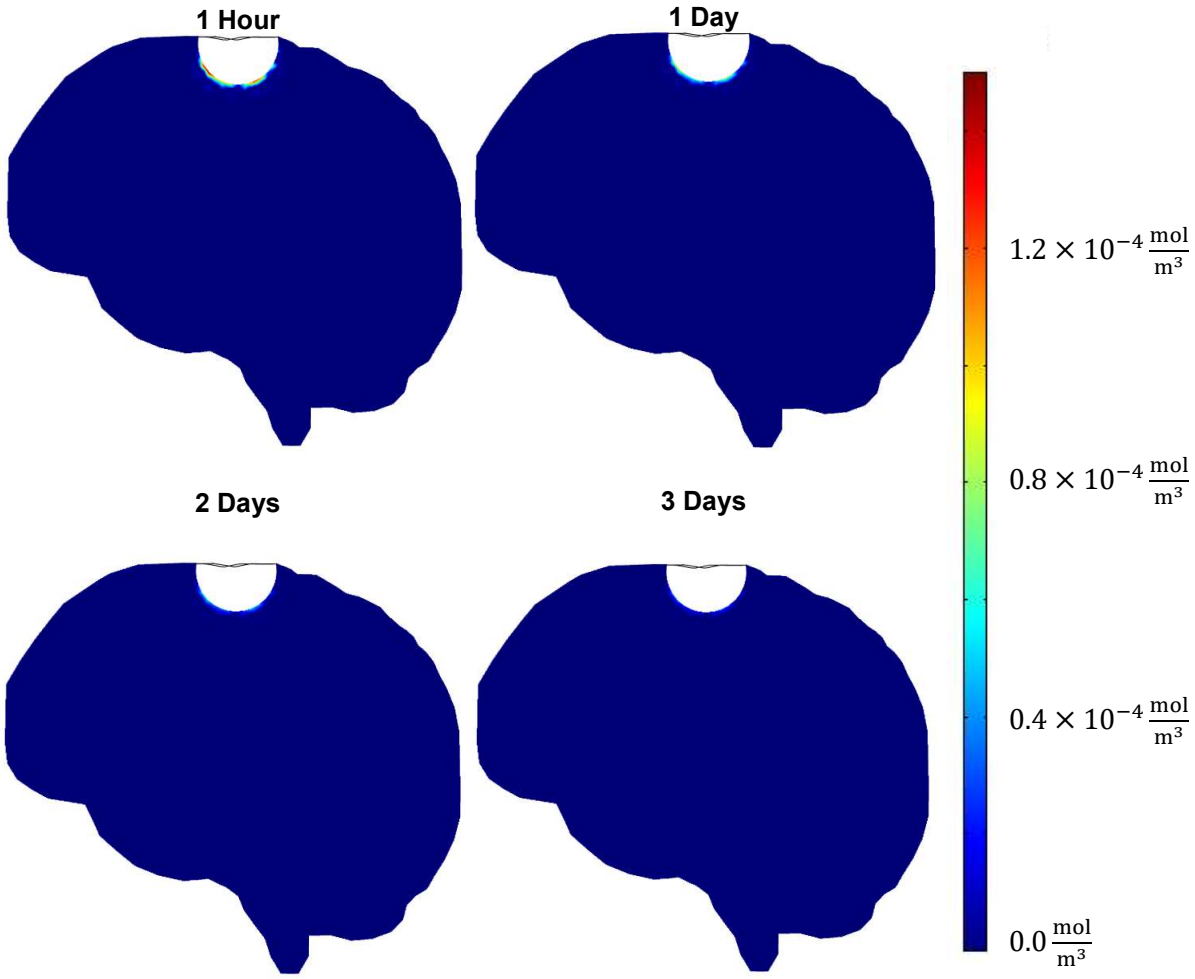


**Figure 8:** Drug concentration in the healthy brain after 1 hour, 1 day, 2 days, and 3 days post-implantation. Concentrations are rather low in most of this region, which means there is minimal damage to the healthy tissue as a result of the carmustine wafers.

Since the majority of the healthy tissue has negligible carmustine concentration at all times shown, the images from Figure 8 have been zoomed in and shown in Figure 9. The maximum concentration of carmustine in the healthy tissue is a full order of magnitude lower than it is in the tumor layer. Since there is significantly less carmustine in the healthy tissue, there will also be significantly less cell death in the healthy tissue.

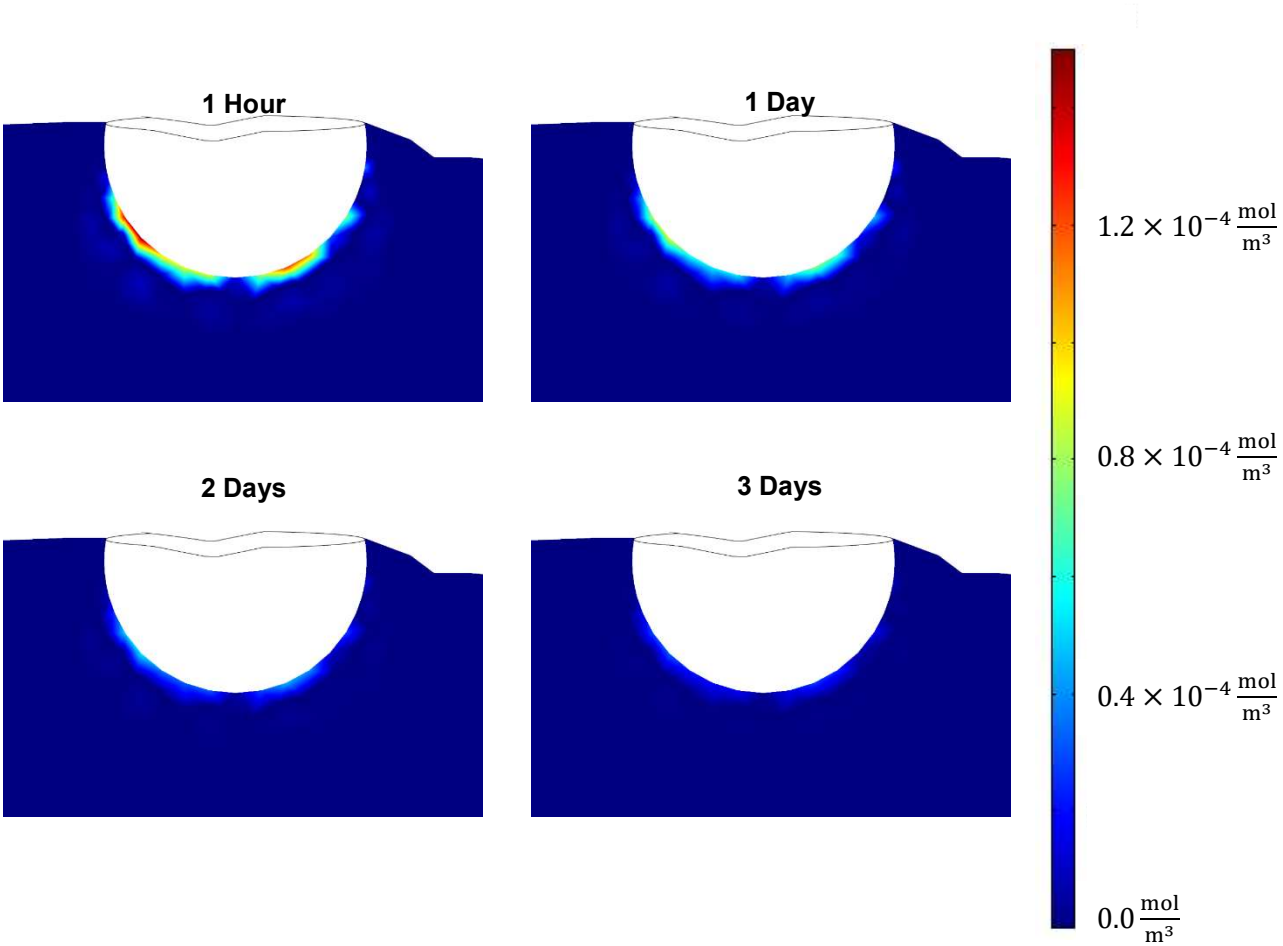


**Figure 9:** Drug rug concentration in the healthy brain after 1 hour, 1 day, 2 days, and 3 days post-implantation. These images are the same as those in Figure 8 but zoomed in to show more detail around the boundary between the healthy tissue and tumor region.

*10.3: Fluid Flow in the Brain*

Fluid flow of blood due to capillaries in the brain is pressure driven. Figure 10 displays a contour map of pressure throughout the brain. As should be expected, the pressure increases linearly with depth.

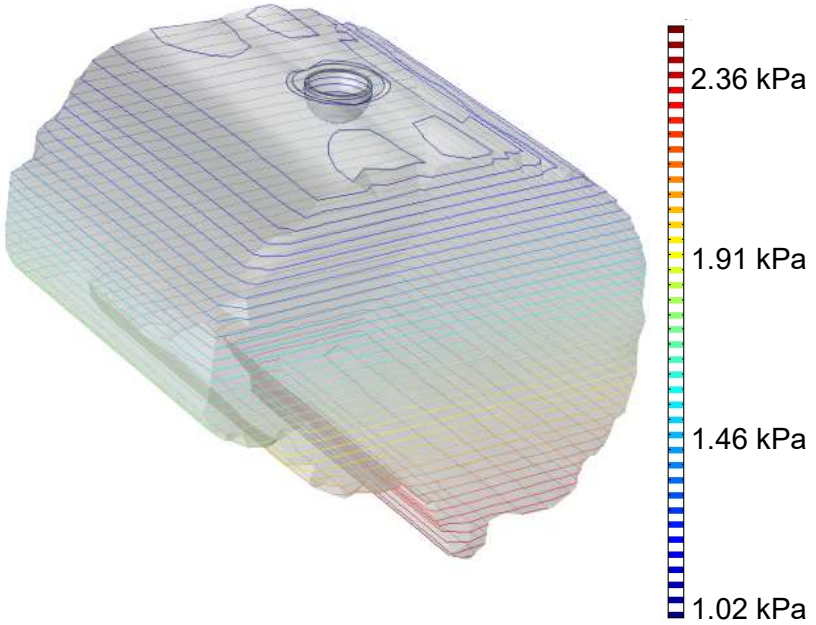


**Figure 10:** Pressure contours in the brain. Pressure increases linearly with depth of the tissue. Fluid flow in the brain is pressure driven.

The fluid flow in the brain is maintained at a steady state. Figure 11 displays the magnitude of the blood's velocity in meters per second through the healthy tissue and tumor region. Blood flow is fastest in most elevated parts of the tumor region and slowest in the healthy tissue. Figure 12 shows the velocity field throughout the brain, demonstrating the velocity direction and relative magnitude.

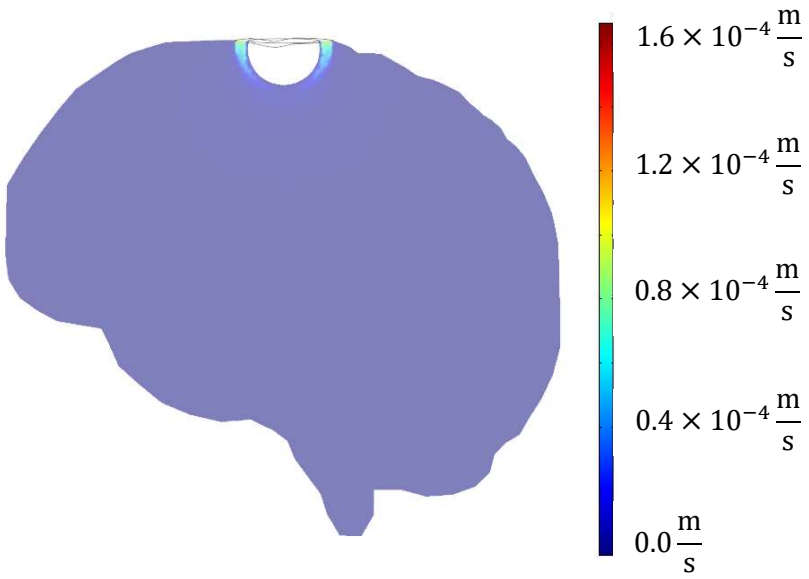


**Figure 11:** Velocity magnitude of blood in the brain. Velocity is highest in the tumor region and very low in the healthy tissue.

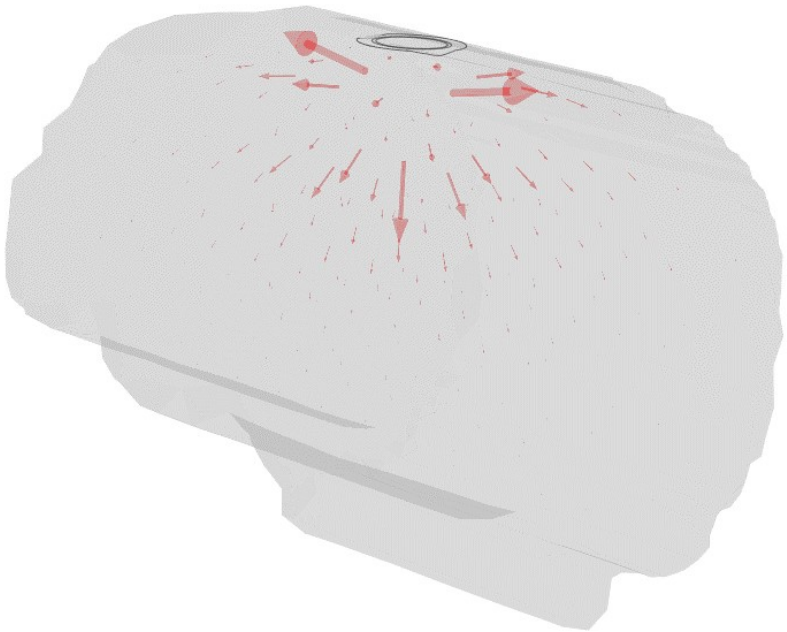

**Figure 12:** Velocity field of blood flow in the brain tissues. Velocity radiates outward from the tumor layer.

*10.4 Data Validation*

As demonstrated in our mesh convergence analysis above, the concentration of carmustine at the cut point (Figure 3) in the tumor layer was proven to fluctuate around a concentration of 13.6 μmol/$m^3$, or $2.92\times10^{-9}$ mg/$mm^3$ (Figure 4). When comparing our cut point carmustine concentration to a similar study done in two dimensions (Brendel, Casey, Gilbert, & Spinella, 2013), data presented in this study is validated. In the Brendel, Casey, Gilbert and Spinella study, the average carmustine concentration at about 1.75 cm from the wafer surface was in the order of $10^{-9}$ mg/$mm^3$. The similarity in magnitude of carmustine concentration in the tumor region between our study and Brendel, Casey, Gilbert, and Spinella's study validates the results of our model.

Another model, using the computational fluid dynamics software Fluent, found the carmustine concentration to be between $1.28 \times 10^{-11}$ and $2.18 \times 10^{-12}$ mol/$cm^3$ in the tumor region (Teo, et al., 2005). The concentration at our cut point (Figure 3) in the tumor layer of 13.6 μmol/$m^3$, which is equivalent to $1.36 \times 10^{-11}$ mol/$cm^3$ is very near to this range. Agreement between our model and Teo's provides further validation for the accuracy of our results.

*10.5 Sensitivity Analysis*

All of the parameters for the governing equations used in our model were obtained experimentally. Since we did not need to estimate any values, we will not be doing sensitivity analysis to identify error that arose from choosing parameter values.

We performed sensitivity analysis to determine how the fitted parameters for the carmustine source in the wafers affect the diffusion of carmustine and how they can be manipulated to allow for optimal treatment (maximizing residence time in the tumor region and minimizing any diffusion into the healthy tissue). We chose these fitted parameters – $S_0$ and $\tau$ – because they can be physically changed relatively easily. All other values pertain to properties of a person's brain and therefore cannot be altered. Sensitivity analysis was only performed with respect to carmustine diffusion because the parameters we will be testing affect only diffusion (since there is only one-way coupling between diffusion and fluid flow).

Physically, the parameter $S_0$ can be changed by altering the initial concentration of carmustine in the wafers. We performed sensitivity analysis to test the effect of $S_0$ on the average tumor region concentration using the $S_0$ determined by Teo, et al. (2005) scaled by factors of 0.1, 1, 5, and 10. As can be seen in Figure 13, average carmustine concentration in the tumor peaks rapidly and then steadily declines. Scaling $S_0$ makes the peak scale by an approximately equal amount. It could be beneficial to create the wafers with higher initial concentrations of carmustine. This would result in higher drug concentrations in the tumor, which would in turn result in higher rates of tumor cell death. Damage to healthy tissue appears to be minimal at the presently used value of $S_0$ due to the very low carmustine concentrations in the region (Figure 9), so this increase should not be very harmful to a patient.

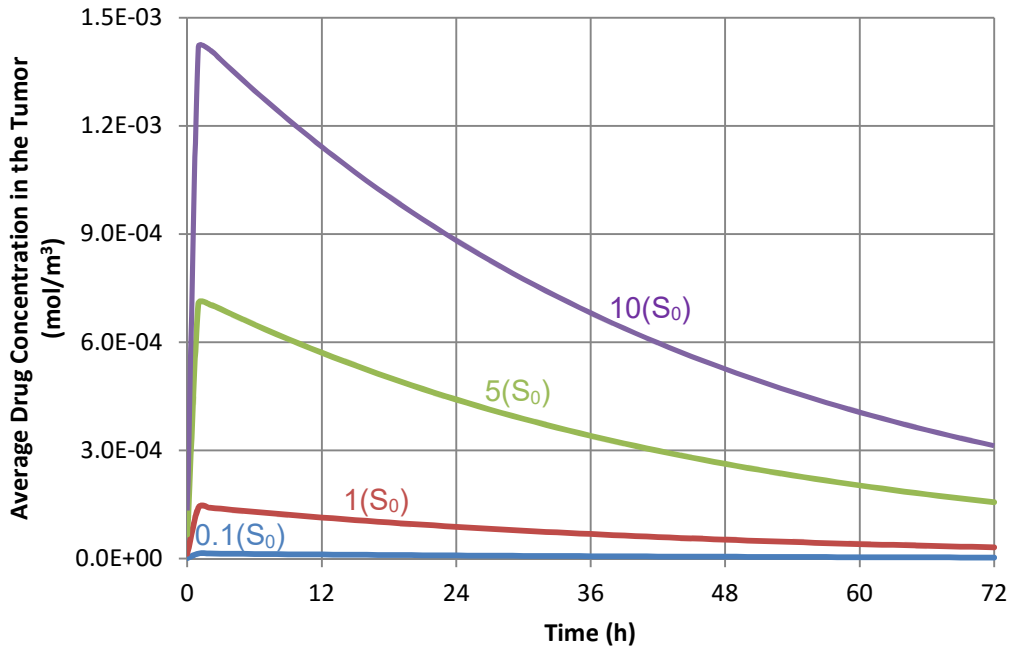


**Figure 13:** Sensitivity analysis on $S_0$ with respect to the average carmustine concentration in the tumor over three days. Increasing $S_0$ increases the average tumor concentration. The general shape of the curve remains the same, though, quickly reaching a peak and steadily declining.

The wafers hold carmustine in a biodegradable matrix and release it as they are eroded away over time. By using a different material, the parameter $\tau$ – a time constant for this erosion – can be changed. We performed sensitivity analysis to test the effect of $\tau$ on the average tumor region concentration using the $\tau$ determined by Teo, et al. (2005) scaled by factors of 0.1, 1, 5, and 10 (Figure 14). Increasing $\tau$ leads to some increase in the maximum average concentration, though its effect is much less significant than $S_0$'s. The more relevant effect $\tau$ has is slowing the decline of the average concentration. Using a material for the wafer with a higher $\tau$ could be beneficial as it would result in prolonged concentration of carmustine in the tumor and, as a result, more tumor cell death.

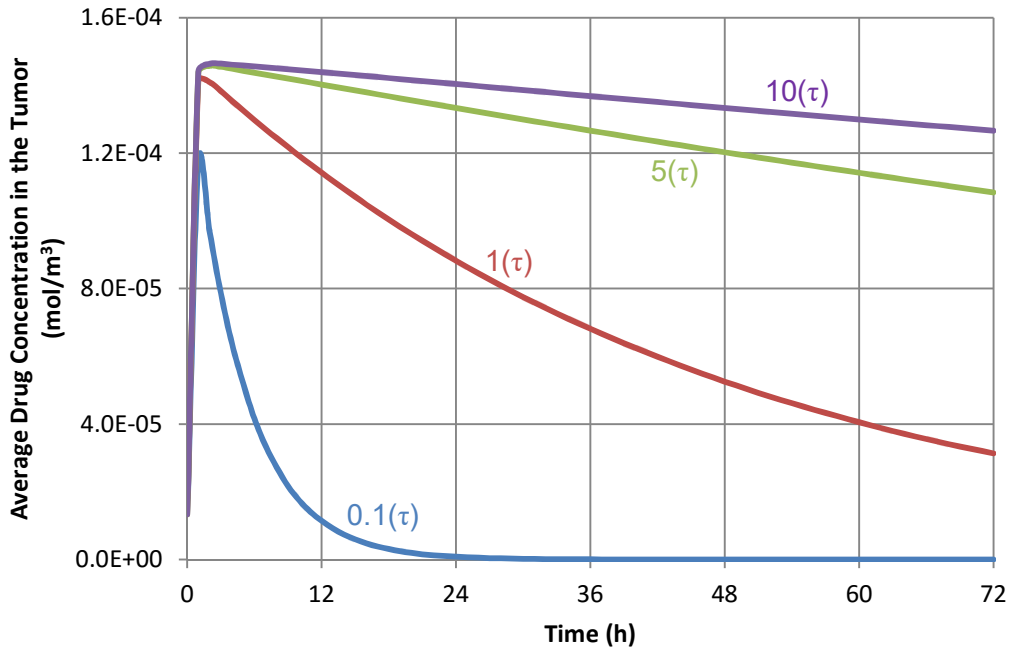


**Figure 14:** Sensitivity analysis on τ with respect to the average carmustine concentration in the tumor over three days. Increasing τ has some effect on the maximum average concentration. The most significant effect is the slower decline in concentration at higher values of τ.

## 11: Conclusions and Future Considerations

Significant cell death begins at carmustine concentrations of 100 μM, or 0.1 mol/m$^3$. The proportion of cells that die rises with the concentration, reaching 80% of cells killed between 500 and 1000 μM, or between 0.5 and 1 mol/m$^3$ (An, et al., 2011). As the maximum carmustine concentration reached in the healthy tissue was $1.5 \times 10^{-4}$ mol/m$^3$ (Figure 8), there is virtually no healthy cell death. However, there is no noticeable cancer cell death either, as the maximum concentration in the tumor layer is $3.5 \times 10^{-3}$ mol/m$^3$ (Figure 7). These numbers demonstrate that the Gliadel wafer treatment does not harm the patient's healthy brain tissue but also does not have the desired effect on cancerous tissue. We propose to overcome this limitation by altering the wafer properties – $S_0$ and τ – to maximize the concentrations reached in the tumor layer while still maintain the maximum concentration in the healthy tissue below the 0.1 mol/m$^3$ concentration threshold for cell death.

By increasing $S_0$ to $1.1318 \times 10^{-2}$ kg/m$^3$s (20 times its original value) and τ to $1.667 \times 10^6$ seconds (10 times its original value) in our simulation, we were able to achieve a maximum carmustine concentration of 0.14 mol/m$^3$ in the tumor layer and keep the concentration elevated above 0.1 mol/m$^3$ for effectively the whole three days of simulation (Figure 15). Alterring $S_0$ and τ in this way would allow for the Gliadel treatment to kill more cancerous cells and potentially be much more effective.

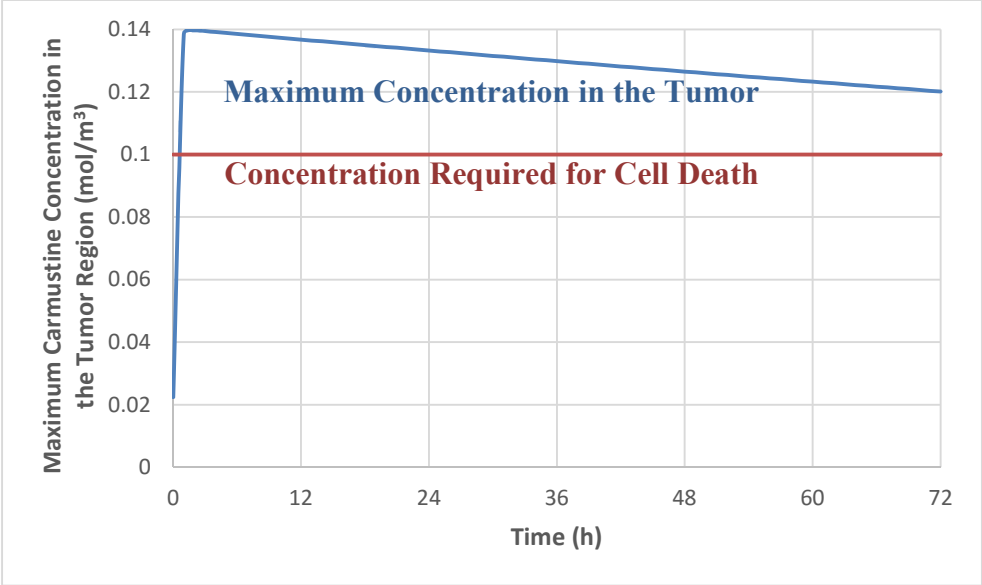


**Figure 15:** Maximum carmustine concentration in the tumor layer with the heightened values of $S_0$ and $\tau$. The concentration exceeds the minimum amount required for cell death early on in the Gliadel treatment and remains above the threshold for over three days.

Additionally, the maximum carmustine concentration in the healthy tissue reached a maximum of only 0.004 mol/m$^3$ (Figure 16). This concentration is significantly lower than the 0.1 mol/m$^3$ threshold, meaning that even with the increased values of $S_0$ and $\tau$ healthy cells are not being killed by carmustine. Increasing the parameters in this way allows us to reach our modelling goal of maximizing the intended effects of the Gliadel treatment while minimizing damage to healthy tissue.

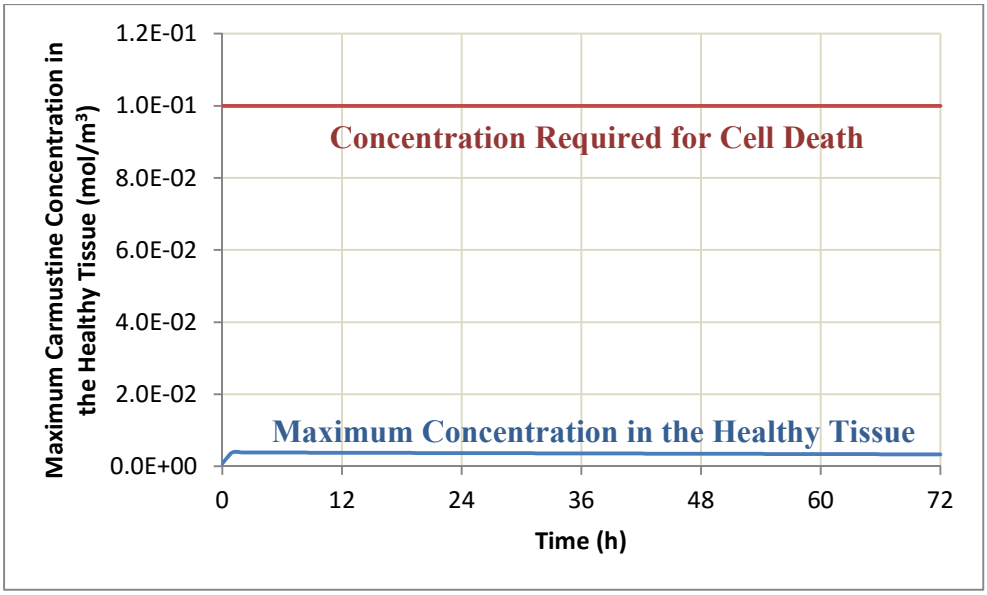


**Figure 16:** Maximum carmsutine concentration in the healthy tissue with the heightened values of $S_0$ and $\tau$. The concentration is significantly lower than the threshold for cell death, so healthy cells are not being harmed by the Gliadel treatment.

We suggest that the Gliadel wafers are altered such that their properties reflect those that we discussed above. $S_0$ could be increased by increasing the amount of carmustine in each wafer and $\tau$ could be increased by using a different material that would degrade more slowly. Gliadel wafers are currently made of a polyanhydride copolymer and the degradation rate could be decreased (effectively increasing $\tau$) by using a more hydrophobic monomer (Kumar, Langer, & Domb, 2002). If Gliadel wafers could be made to these specifications, the treatment would be more effective and could possibly prolong life expectancy of glioblastoma multiforme patients.

**12: Acknowledgments**

We would like to thank Alexander Warning for his support and help using the COMSOL software, Traci Nathans-Kelly for reviewing and critiquing this report, and the Academic Computing Center in the Engineering Library (ACCEL) at Cornell University for providing computers COMSOL licenses.

**13: References**

An, J., Kim, S., Rhie, J., Shin, D., Seo, S., & Seo, J. (2011). Carmustine induces ERK- and JNK-dependent cell death of neuronally-differentiated PC12 cells via generation of reactive oxygen species. *Toxicology in Vitro, 25*(7), 1359-1365. Retrieved from http://www.sciencedirect.com/science/article/pii/S0887233311001317?np=y.

Baxter, L. T., & Jain, R. K. (1989). Transport of fluid and macromolecules in tumors. Role of interstitial pressure and convection. *Microvascular Research*, *37*(1), 77-104.

Brendel, M., Casey, M., Gilbert, R., & Spinella, M. (2013). Chemotherapuetic Treatment Using Controlled Drug Delivery of BCNU via Nanoparticles. Retrieved from https://ecommons.cornell.edu/bitstream/handle/1813/33347/Group%206-%20Final%20Project%20Report.pdf?sequence=2&isAllowed=y.

Brennan, J., Colangelo, N., Pendery, L., & Skeans, W. (2009). Convection Enhanced Drug Delivery for the Treatment of Brain Gliomas. Retrieved from https://ecommons.cornell.edu/bitstream/handle/1813/12644/2009BEE4530_Group1_FinalReport.pdf?sequence=1&isAllowed=y.

Chudler, E. (2016). Brain Facts and Figures. Retrieved from https://faculty.washington.edu/chudler/facts.html#brain.

Dyke, J., Sanelli, P., Voss, H., Serventi, J., Stieg, P., Schwartz, T., & Pannullo, S. (2007). Monitoring the effects of BCNU chemotherapy Wafers (Gliadel) in glioblastoma multiforme with proton magnetic resonance spectroscopic imaging at 3.0 Tesla. *Journal of Neuro-Oncology*, *82*(1), 103-110. Retrieved from http://link.springer.com/article/10.1007/s11060-006-9254-6?no-access=true.

Fleming, A., Saltzman, W. (2012). Pharmacokinetics of the Carmustine Implant. *Clinical Pharmacokinetics, 41*(6), 403-419. Retrieved from http://link.springer.com/article/10.2165/00003088-200241060-00002.

Fung, L., Ewend, M., Sills, A., Sipose, E., Thompson, R., Watts, M., & Saltzman, W. (1998). Pharmacokinetics of interstitial delivery of carmustine, 4-hydroperoxycyclophosphamide, and paclitaxel from a biodegradable polymer implant in the monkey brain. *Cancer Res*, *58*(40), 672-684. Retrieved from http://cancerres.aacrjournals.org/content/58/4/672.long.

Goodman, Gilman, A., Rall, T.W., Nies, A. S., & Taylor, P., 1990. Goodman and Gilman's The Pharmacological Basis of Therapeutics, Eighth ed. Pergamon Press, New York, p. 1221.

Holland, E. C. (2000). Glioblastoma multiforme: The terminator. *Proceedings of the National Academy of Sciences of the United States of America*, *97*(12), 6242–6244. Retrieved from http://www.ncbi.nlm.nih.gov/pmc/articles/PMC33993/.

Kenhub. (2016). Lateral View of the Brain. Retrieved from https://www.kenhub.com/en/library/anatomy/lateral-view-of-the-brain.

Kumar, N., Langer, R., & Domb, A. (2002). Polyanhydrides: an overview. *Advanced Drug Delivery Reviews, 54*(7), 889-910.

Levin, V. A., Stearns, J., Byrd, A. N. N. E., Finn, A., & Weinkam, R. J. (1979). The effect of phenobarbital pretreatment on the antitumor activity of 1, 3-bis (2-chloroethyl)-1-nitrosourea (BCNU), 1-(2-chloroethyl)-3-cyclohexyl-1-nitrosourea (CCNU) and 1-(2-chloroethyl)-3-(2, 6-dioxo-3-piperidyl-1-nitrosourea (PCNU), and on the plasma pharmacokinetics and biotransformation of BCNU. *Journal of Pharmacology and Experimental Therapeutics*, *208*(1), 1-6.

Loo, T., Dion, R., Dixon, R., & Rall, D. (1966). The Antitumor Agent, 1,3-bis(2-chloroethyl)-1-nitrosourea. *Journal of Pharmaceutical Sciences, 55*(5), 492-497.

Panigrahi, M., Das, P., & Parikh, P. (2011). Brain tumor and Gliadel wafer treatment. *Indian Journal of Cancer*, *48*(1), 11-17. Retrieved from http://www.indianjcancer.com/article.asp?issn=0019-509X;year=2011;volume=48;issue=1;spage=11;epage=17;aulast=Panigrahi.

Perry, R.H. (Ed), 1997. Perry's Chemical Engineers' Handbook. McGraw-Hill, New York, pp. 2.94–2.98.

RxList. (2013). Gliadel. Retrieved from http://www.rxlist.com/gliadel-drug.htm.

RxList. (2013). Gliadel Side Effects Center. Retrieved from http://www.rxlist.com/gliadel-side-effects-drug-center.htm.

Saltzman, W. M., & Radomsky, M. L. (1991). Drugs released from polymers: diffusion and elimination in brain tissue. *Chemical Engineering Science*, *46*(10),

Teo, C. S., Tan, W. H. K., Lee, T., & Wang, C. H. (2005). Transient interstitial fluid flow in brain tumors: Effect on drug delivery. *Chemical Engineering Science*, *60*(17), 4803-4821.

Wang, C., Li, J., Teo, C., & Lee, T. (1999). The delivery of BCNU to brain tumors. *J Control Release*, *61*(1), 21-41. Retrieved from http://www.ncbi.nlm.nih.gov/pubmed/10469900.

Weber, E., & Goebel, E. (2005). Cerebral edema associated with Gliadel wafers: Two case studies. *Neuro-oncol*, *7*(1), 84-89. Retrieved from http://www.ncbi.nlm.nih.gov/pmc/articles/PMC1871626/.

Westphal, M., Ram, Z., Riddle, V., & Bortey, E. (2006). Gliadel wafer in initial surgery for malignant glioma: long-term follow-up of a multicenter controlled trial. *Acta Neurochirurgica*, *148*(3), 269-275. Retrieved from http://link.springer.com/article/10.1007/s00701-005-0707-z.

Wooding, R. A. (1957). Steady state free thermal convection of liquid in a saturated permeable medium. *Journal of Fluid Mechanics*, *2*(03), 273-285.